Phonon dispersion and specific heat of Graphene in the context of magnetocaloric applications

Alvaro Herrera[1], Carlos Colchero[2], Abiel Galindo[3], Jose Carrandi[4] and Jorge Perez[5]

[1] *A00836274@tec.mx*
[2] *A00835489@tec.mx*
[3] *A00836342@tec.mx*
[4] *A01722194@tec.mx*
[5] *A00835537@tec.mx*

F2007B - Analysis of thermodynamic and statistical systems (Group 601).
Professor: Hector Medel, PhD.
December 1, 2024.

Abstract—The main objective of this work is to obtain mathematical models for the specific heat of a graphene lattice subject to neighbor interactions and an external magnetic field. Furthermore, the future implementations of these models are discussed as related to the magnetocaloric effect. A second neighbor interaction model is constructed through the calculation of the dynamic matrix of the system, and an efficient Ising model is designed to describe the magnetic interactions within the lattice.

Keywords—graphene, specific heat, magnetocaloric effect, Ising model, magnetic hyperthermia, phonons, first neighbors, second neighbors.

I. Introduction

Throughout this work, an analytical and numerical analysis of the behavior of graphene is developed. The mathematical framework necessary to describe the phononic interactions within Graphene's lattice are presented, and their implications on the physical characteristic of Graphene-based materials are discussed. The main aim of this work is to provide a complete description of Graphene's specific heat in the presence of an external magnetic field.

In order to do so, the neighbor interactions within the graphene lattice are defined through a Coulomb potential. Furthermore, Bragg's diffraction theory is explored, studying the relation between incident light and phononic interactions within the material. Finally, the internal energy of the lattice is recovered, allowing for the calculation of the lattice's specific heat.

Additionally, the specific heat of Graphene due to magnetic interactions is explored. For these purpose, an efficient Ising algorithm is constructed, allowing for an in depth study of the variations in the specific heat of a hexagonal lattice in the presence of an external magnetic field.

The complete description of graphene's specific heat allows for a better understanding of the material's reaction to changes in temperature and external magnetic field. This understanding is fundamental for the implementation of ferromagnetic graphene alloys in magnetocaloric systems. In future projects, more complicated graphene alloys will be modelled, allowing for a characterization of important materials used in modern magnetocaloric applications, such as cancer treatment or refrigeration.

II. Methodology

a. Principles of Solid State Physics

Solid state physics primarily deals with materials with periodically arranged atomic or molecular constituents. This well-defined periodic pattern is known as a crystal lattice; the Solid State model describes a solid through the use of an infinite dimensional lattice in 3D space, which holds translational symmetry. Mathematically, a lattice can be expressed as:

$$\vec{R}_n = n_1\vec{a}_1 + n_2\vec{a}_2 + n_3\vec{a}_3 \tag{1}$$

The set of vectors $\{\vec{a}_i\}_{i=1}^{3}$ is known as the primitive vector set. They define the primitive lattice, which is the smallest repeating translational unit of the crystal lattice. In the study of Bravais lattices, the linear combination described in (1) must also ensure that $n_i \in \mathbf{Z}$. To construct the primitive lattice, one must identify the specific geometry of the minimum cell such that, through repeated translation, it correctly fills the entire lattice space. This cell is known as the primitive cell, and will be discussed again later.

Therefore, the primitive vectors are not unique, and should be determined based on the symmetry of the crystal.

Another useful concept in solid state physics is the basis or motif of the lattice. Previously, the primitive lattice (also known as primitive cell) was defined. The primitive lattice captures the symmetry and periodicity of the crystal, but lacks information regarding the atomic and molecular arrangement within the solid.

The motif describes this molecular arrangement, by associating a group of atoms, ions, or molecules with each lattice point. The motif specifies the local arrangement of atoms, ions, or molecules at each one of the lattice points. To construct a motif, it is necessary to specify the number of atoms and the type of atoms to fully reproduce the original material's structure.

Once the primitive lattice has been defined, it is possible to construct a primitive cell. The primitive cell is defined as the smallest volume of space such that, when tessellated, it completely reproduces the primitive lattice with no gaps. In this project, the primitive cell that will be utilized is known as the **Wigner Cell**. The Wigner Cell is constructed around one point of the lattice, and must reproduce the entire lattice when tessellated.

Throughout this project, Graphene's lattice structure will be thoroughly analyzed. Graphene has a monatomic, hexagonal lattice; therefore, the motif consists of a single element, while the Wigner cell will be hexagonal.

b. Bragg's Law

To develop a comprehensive understanding of the lattice dynamics in crystalline materials like graphene, it is essential to first explore the structural characterization of the lattice through diffraction techniques. This foundation allows for a dynamic description of the elements within the lattice. In order to describe how each element within the lattice reacts to interactions with external agents, Bragg diffraction must be explored.

Bragg's law describes the relationship between the incident electromagnetic wave and the periodic structure of the crystal lattice. Whenever an incident photon interacts with an element in the lattice, a vibrational reaction transpires. Particular electromagnetic waves, with appropriate values of the wave vector, result in constructive interference.

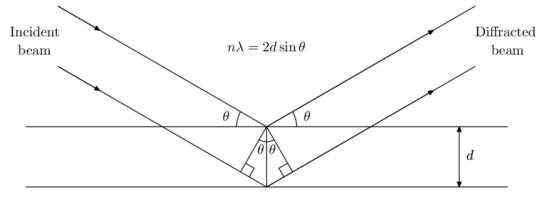

Fig. 1: Bragg's Law Diagram

The expression for the appropriate incident wave vectors is given by:

$$2d\sin\theta = n\lambda, \tag{2}$$

where d is the distance between parallel planes in the crystal lattice, θ is the angle of the incoming beam, n is an integer (order of reflection), and λ is the wavelength of the incident wave. Therefore, the path difference between waves scattered from consecutive planes must be an integer multiple of the wavelength for constructive interference.

An important assumption in the analysis of diffraction is that energy must be conserved, which implies that the magnitudes of the incident and scattered wave vectors are the same:

$$|\mathbf{k}| = |\mathbf{k}'| = \frac{2\pi}{\lambda}. \tag{3}$$

Here, $\mathbf{k}$ is the wave vector of the incident wave, and $\mathbf{k}'$ is the wave vector of the scattered wave. Evidently, the wavelength, and thus the energy, of the incoming wave is preserved during the scattering process.

Considering the change in momentum during the scattering process, the condition for constructive interference can be rewritten in terms of the wave vectors as:

$$\mathbf{G} = \mathbf{k}' - \mathbf{k}, \tag{4}$$

where $\mathbf{G}$ is a reciprocal lattice vector. This equation implies that the difference between the incident and scattered wave vectors corresponds to a vector in the reciprocal lattice. The reciprocal lattice vector $\mathbf{G}$ satisfies the condition:

$$\mathbf{G}\cdot(\mathbf{R}_n - \mathbf{R}_0) = 0, \tag{5}$$

where $\mathbf{R}_n$ represents a lattice vector in real space, defined as:

$$\mathbf{R}_n = \sum_{i=1}^{3} n_i \mathbf{a}_i, \tag{6}$$

with $n_i \in \mathbb{Z}$ being integers and $\mathbf{a}_i$ the primitive vectors of the Bravais lattice. This condition states that the vector $\mathbf{G}$ is orthogonal to the vector $\mathbf{R}_n - \mathbf{R}_0$; this equation is similar to the equation of a plane:

$$\mathbf{n}\cdot(\mathbf{r} - \mathbf{r}_0) = 0, \tag{7}$$

where $\mathbf{n}$ is the normal vector to the plane. In this context, $\mathbf{G}$ acts as the normal vector defining the orientation of the lattice planes, often referred to as Bragg planes.

The diffraction pattern obtained from experiments provides information about the reciprocal lattice, a conceptual space where the periodicity of the crystal is represented by vectors $\mathbf{G}$. The reciprocal lattice is defined such that any vector $\mathbf{G}$ satisfies:

$$\mathbf{G}\cdot\mathbf{R} = 2\pi n, \quad \text{for any lattice vector } \mathbf{R}. \tag{8}$$

The Bragg condition in reciprocal space can be restated as:

$$\mathbf{d}\cdot(\mathbf{k}' - \mathbf{k}) = n\lambda \quad \Longrightarrow \quad \mathbf{d}\cdot\mathbf{G} = 2\pi n, \tag{9}$$

where $\mathbf{d}$ is the vector normal to the lattice plane, and $\mathbf{G}$ represents the wave vector corresponding to the periodicity of the lattice in reciprocal space.

To construct the reciprocal lattice, we use the basis vectors:

$$\mathbf{b}_1 = 2\pi \frac{\mathbf{a}_2 \times (\mathbf{a}_1 \times \mathbf{a}_2)}{|\mathbf{a}_1 \times \mathbf{a}_2|^2}$$
$$\mathbf{b}_2 = 2\pi \frac{\mathbf{a}_1 \times (\mathbf{a}_2 \times \mathbf{a}_1)}{|\mathbf{a}_1 \times \mathbf{a}_2|^2} \quad (10)$$

The general reciprocal lattice vector can be expressed as:

$$\mathbf{G}_{hkl} = h\mathbf{b}_1 + k\mathbf{b}_2, \quad \{h,k\} \in \mathbb{Z}. \quad (11)$$

These indices provide a way to identify the planes responsible for the observed diffraction peaks. The discrete nature of the reciprocal lattice reinforces the periodicity of the crystal, allowing for the mapping of the wave vectors back to the real-space structure.

A Wigner cell may also be defined in the reciprocal lattice, analogous to the one in real space. This Wigner cell contains the fundamental region of wave vectors and is crucial in understanding the vibrational properties of the lattice. The entire set of allowed wave vectors will be contained in the reciprocal lattice.

Understanding Bragg's law and the reciprocal lattice is essential in the study of harmonic interaction within a material's lattice. The diffraction pattern provides information about the periodic structure of the crystal through the reciprocal lattice vectors. By analyzing the diffraction peaks, the reciprocal lattice is constructed, which in turn allows for the reconstruction of the real-space lattice structure. This step is necessary in modeling interatomic interactions and deriving the equations of motion, as it provides the framework for understanding the vibrational states and dynamics of the crystal.

c. Harmonic Approximation

First off, a harmonic approximation for the potential U between the μ and ξ motifs of the lattice is considered. Each of the motifs within the lattice contains ν and η atoms. Finally, the coordinates for the atoms in both basis will be denoted as α and β.

$$U^{harm}[(\vec{r}_{nk});(\vec{R}_n)] \simeq U_0 + \frac{1}{2}\sum_{\mu\nu\xi\eta\alpha\beta} \frac{\partial^2 U}{\partial r_{\mu\nu\alpha}\partial r_{\xi\eta\beta}}\bigg|_{\vec{R}_0} U_{\mu\nu\alpha}U_{\xi\eta\beta}, \quad (12)$$

Considering interactions between elements of the harmonic lattice, the following expression is obtained:

$$U_{\mu\nu\xi\eta}\left[||(\vec{R}_\mu + \vec{d}_\nu + \vec{u}_{\mu\nu}) - (\vec{R}_\xi + \vec{d}_\eta + \vec{u}_{\xi\eta})||\right]. \quad (13)$$

Since only pairwise interaction is considered:

$$U_{total} = \frac{1}{2}\sum_{\mu\nu\xi\eta} U_{\mu\nu\xi\eta}. \quad (14)$$

Using Hooke's law,

$$U_{\mu\nu\xi\eta} = C_{\mu\nu\xi\eta}\left[\left|\left|\vec{R}_\mu + \vec{d}_\nu + \vec{u}_{\mu\nu} - (\vec{R}_\xi + \vec{d}_\eta + \vec{u}_{\xi\eta})\right|\right| - \left|\left|\vec{R}_\mu + \vec{d}_\nu - \vec{R}_\xi - \vec{d}_\eta\right|\right|\right]^2. \quad (15)$$

Afterward, small displacements will be considered,

$$||\vec{u}_{\mu\nu}|| \ll |||\vec{R}_\mu + \vec{d}_\nu||. \quad (16)$$

Next, let

$$\vec{A} \equiv \vec{R}_\mu - \vec{R}_\xi + \vec{d}_\nu - \vec{d}_\eta + (\vec{u}_{\mu\nu} - \vec{u}_{\xi\eta}), \quad (17)$$
$$\vec{R}_{\mu\nu\xi\eta} \equiv \vec{R}_\mu - \vec{R}_\xi + \vec{d}_\nu - \vec{d}_\eta, \quad (18)$$
$$\vec{u}_{\mu\nu\xi\eta} \equiv \vec{u}_{\mu\nu} - \vec{u}_{\xi\eta}. \quad (19)$$

Thus, equation (17) can be expressed as

$$\vec{A} = \vec{R}_{\mu\nu\xi\eta} + \vec{u}_{\mu\nu\xi\eta} = R_{\mu\nu\xi\eta}\left(\hat{R}_{\mu\nu\xi\eta} + \frac{\vec{\mu}_{\mu\nu\xi\eta}}{R_{\mu\nu\xi\eta}}\right). \quad (20)$$

Hence,

$$||\vec{A}|| = R_{\mu\nu\xi\eta}\left(1 + \frac{2\vec{u}_{\mu\nu\xi\eta}\cdot\hat{R}_{\mu\nu\xi\eta}}{R_{\mu\nu\xi\eta}} + \frac{u^2_{\mu\nu\xi\eta}}{R^2_{\mu\nu\xi\eta}}\right)^{1/2}. \quad (21)$$

Let

$$\varepsilon \equiv \frac{2\vec{u}_{\mu\nu\xi\eta}\cdot\hat{R}_{\mu\nu\xi\eta}}{R_{\mu\nu\xi\eta}}.$$

Thus, by making a Taylor approximation of first order, the following expression is established

$$||\vec{A}|| \simeq R_{\mu\nu\xi\eta}\left(1 + \frac{1}{2}\varepsilon + ...\right)^{1/2}. \quad (22)$$

Therefore, the harmonic potential can be expressed as

$$U^{harm}_{\mu\nu\xi\eta} \simeq C_{\mu\nu\xi\eta}\left(\vec{u}_{\mu\nu\xi\eta}\cdot\hat{R}_{\mu\nu\xi\eta}\right)^2. \quad (23)$$

Considering interaction by pairs, (23) can be written as

$$U^{harm} = \sum_{\mu\nu}\sum_{\xi\eta}\frac{C_{\mu\nu\xi\eta}}{4}\left[\hat{R}_{\mu\nu\xi\eta}\cdot(\vec{u}_{\mu\nu} - \vec{u}_{\xi\eta})\right]^2, \quad (24)$$
$$= \sum_{\mu\nu}\sum_{\xi\eta}\sum_{\alpha\beta}\frac{C_{\mu\nu\xi\eta}}{4}\left(\hat{R}_{\mu\nu\xi\eta\alpha}\hat{R}_{\mu\nu\xi\eta\beta}\right)\left(u_{\mu\nu\alpha}u_{\mu\nu\beta} - u_{\mu\nu\alpha}u_{\xi\eta\beta}\right), \quad (25)$$
$$= \frac{1}{2}\sum_{\mu\nu}\sum_{\xi\eta}\sum_{\alpha\beta}\left\{\left[\sum_{\xi'\eta'} C_{\mu\nu\xi'\eta'}\hat{R}_{\mu\nu\xi'\eta'\alpha}\hat{R}_{\mu\nu\xi'\eta'\beta}\right]\cdot\delta^\mu_\xi\delta^\nu_\eta - C_{\mu\nu\xi\eta}\hat{R}_{\mu\nu\xi\eta\alpha}\hat{R}_{\mu\nu\xi\eta\beta}\right\}u_{\mu\nu\alpha}u_{\xi\eta\beta}, \quad (26)$$
$$= \frac{1}{2}\sum_{\mu\nu}\sum_{\xi\eta}\sum_{\alpha\beta}D^{\mu\nu\xi\eta}_{\alpha\beta}u_{\mu\nu\alpha}u_{\xi\eta\beta}, \quad (27)$$

where

$$D^{\mu\nu\xi\eta}_{\alpha\beta} \equiv \sum_{\xi'\eta'}\left(C_{\mu\nu\xi'\eta'}\hat{R}_{\mu\nu\xi'\eta'\alpha}\hat{R}_{\mu\nu\xi'\eta'\beta}\right)\delta^\mu_\xi\delta^\nu_\eta - C_{\mu\nu\xi\eta}\hat{R}_{\mu\nu\xi\eta\alpha}\hat{R}_{\mu\nu\xi\eta\beta} \quad (28)$$

is the dynamic matrix of the system. It is Hermitian and symmetric. As a consequence, conservation of energy dictates

$$\sum_{\xi\eta} D_{\alpha\beta}^{\mu\nu\xi\eta} = 0. \tag{29}$$

Subsequent, the kinetic energy of the system can be written as

$$T = \frac{1}{2} m \sum_{abc} \dot{u}_{abc}^2. \tag{30}$$

Hence, the equations of motion can be obtained using Euler-Lagrange equation

$$\frac{d}{dt}\left(\frac{\partial \mathscr{L}}{\partial \dot{u}_{\mu\nu\alpha}}\right) = \sum_{abc} (m\ddot{u}) \delta_{\mu\nu\alpha}^{abc}, \tag{31}$$

$$= \frac{\partial U^{harm}}{\partial u_{\mu\nu\alpha}}, \tag{32}$$

$$= \frac{1}{2} \sum_{abc} \sum_{\xi\eta\beta} D_{\alpha\beta} \left[\delta_{\mu\nu\alpha}^{abc} \left(u_{\xi\eta\beta}\right) + \delta_{\mu\nu\alpha}^{\xi\eta\beta} \left(u_{abc}\right) \right], \tag{33}$$

$$= \frac{1}{2} \sum_{\xi\eta\beta} D_{\alpha\beta} (u_{\xi\eta\beta}). \tag{34}$$

Thus,

$$\sum_{\mu\nu\alpha} (m\ddot{u}_{\mu\nu\alpha}) \delta_{abc}^{\mu\nu\alpha} = \sum_{\xi\eta\beta} D_{\alpha\beta} (u_{\xi\eta\beta}). \tag{35}$$

Since coupled oscillators are being considered, a solution of the following form is proposed:

$$u_{\mu\nu\alpha}(t) = \sum_{\vec{k}\omega} \varepsilon_x exp\left[i \left(\vec{k} \cdot \vec{R}_{\mu\nu} - \omega t \right) \right]. \tag{36}$$

Incorporating equation (36) in (35),

$$\frac{\partial U}{\partial u_{\mu\nu\alpha}} = \sum_{\mu\nu\alpha} \sum_{\vec{k}\omega} (-\omega^2 m \varepsilon_\alpha) \delta_{abc}^{\mu\nu\alpha} exp\left[i \left(\vec{k} \cdot \vec{R}_{\mu\nu} \right) \right] \tag{37}$$

$$= \sum_{\xi\eta\beta} \sum_{\vec{k}\omega} D_{\alpha\beta} \varepsilon_\beta exp\left[i \left(\vec{k} \cdot \vec{R}_{\xi\eta} \right) \right]. \tag{38}$$

Rearranging terms,

$$\sum_{\vec{k}\omega} \varepsilon_c \exp(i\vec{k} \cdot \vec{R}_{ab}) = \sum_{\vec{k}\omega} \sum_{\xi\eta\beta} D_{\alpha\beta} \exp(i\vec{k} \cdot \vec{R}_{\xi\eta}), \tag{39}$$

$$\sum_{\vec{k}\omega} \Big[-\omega^2 m \varepsilon_c \exp(i\vec{k} \cdot \vec{R}_{ab}) - \sum_{\xi\eta\beta} D_{\alpha\beta} \varepsilon_\beta \exp(i\vec{k} \cdot \vec{R}_{\xi\eta}) \Big] = 0, \tag{40}$$

$$\sum_{\vec{k}\omega} \sum_{\beta} \Big[-\omega^2 m \varepsilon_\beta \delta_c^\beta \exp(i\vec{k} \cdot \vec{R}_{ab}) - \sum_{\xi\eta} D_{\alpha\beta} \varepsilon_\beta \exp(i\vec{k} \cdot \vec{R}_{\xi\eta}) \Big] = 0, \tag{41}$$

$$\Big[-(\omega^2 m) \delta_c^\beta - \sum_{\xi\eta} D_{\alpha\beta} \exp(i\vec{k} \cdot \vec{R}_{ab\xi\eta}) \Big] \varepsilon_\beta = 0. \tag{42}$$

Evidently, equation (42) is a characteristic equation with $3Np$ roots. Thus, there exist $3Np$ vibrational frequencies, which define the dispersion relations $w(k)$, where k is the wave number.

Furthermore, a diagonalization procedure on (42) is performed by letting

$$Q_{\xi\eta\beta} \equiv A_{\xi\eta\beta} e^{i\omega_{\xi\eta\beta} t}, \tag{43}$$

and returning to the original coordinate system

$$u_{\nu\kappa\alpha}(t) = \sum_{\delta\gamma\xi} A_{\xi\eta\beta} \left(A_{\mu\nu\alpha}^{\xi\eta\beta} \right) e^{i\omega_{\xi\eta\beta} t}. \tag{44}$$

Finally,

$$u_{\nu\kappa\alpha}(t) = \sum_{\vec{k},\omega} \frac{\sqrt{N m_{\nu\kappa}}}{N m_{\nu\kappa}} \varepsilon_{\kappa\alpha}(\vec{k}) e^{i\left[\vec{k} \cdot \vec{R}_{\nu\kappa} - \omega(\vec{k}) t\right]}. \tag{45}$$

where $\varepsilon_{\kappa\alpha}$ provides information on the amplitude. In the next section, the aforementioned methodology will be replicated to obtain the allowed angular frequencies for a graphene hexagonal lattice.

d. Solid State analysis of Graphene

Throughout this work, the general framework of solid state physics for periodic lattices has been introduced. One of the fundamental parts of this treatment is the mathematical description of neighbor interactions. This was achieved through the definition of a harmonic potential, U^{harm}, which was then introduced to the Lagrangian of the lattice. By solving Euler-Lagrange's equations of motion, the solution to the displacement of each of the elements in the lattice was found.

As previously stated, the solution to the displacement of each element within the lattice was found in terms of the wave vector and the angular frequency. Furthermore, the characteristic equation was established, which will serve useful in finding the allowed angular frequencies of vibration within the lattice.

Before focusing on Graphene, it deems important to further explore the characteristic equation (42). This equation contains the dynamical description of the lattice, encoded within the **dynamical matrix** and the angular frequencies squared (also known as phonon frequencies) of the lattice. The displacement of an element in the lattice was found to be described by (45).

Clearly, it is necessary to find the appropriate wave vectors and allowed angular frequencies to properly describe the displacement of elements in the lattice. In order to do so, the characteristic equation (42) can be expressed in matrix form:

$$\mathbf{det}(D_{\delta,\gamma,\xi,\mu,\lambda,\beta} - \omega^2 \hat{I}) = 0. \tag{46}$$

When solving the characteristic equation, the allowed values for the angular frequencies will be established. However, to find the allowed wave vectors, it is necessary to set boundary conditions. Throughout this work, periodic boundary conditions will be implemented. The periodic, or Born-von Karman, boundary conditions, are defined for a lattice with N_i unit cells along the direction of a primitive vector a_i:

$$u(\vec{r}+N_i\vec{a}_i,t)=u(\vec{r},t). \tag{47}$$

The main takeaway from this fact is that, whenever the displacement of the element of the lattice has a phase of the form:

$$u(\vec{r},t)\alpha\ e^{i(\vec{k}\cdot\vec{r}-\omega t)}, \tag{48}$$

it is possible to discretize the values of $\vec{k}$. By applying the Born-von Kármán conditions to (48), the restriction is found to be:

$$e^{i(\vec{k}\cdot\vec{a}_iN_i)}=1. \tag{49}$$

Recalling the previous treatment of reciprocal space in b, where the definition of the reciprocal basis vectors was given to be [1]:

$$\begin{aligned}\mathbf{b}_1&=2\pi\frac{\mathbf{a}_2\times(\mathbf{a}_1\times\mathbf{a}_2)}{|\mathbf{a}_1\times\mathbf{a}_2|^2},\\ \mathbf{b}_2&=2\pi\frac{\mathbf{a}_1\times(\mathbf{a}_2\times\mathbf{a}_1)}{|\mathbf{a}_1\times\mathbf{a}_2|^2},\end{aligned} \tag{50}$$

it is possible to describe the wave vector in the reciprocal basis as:

$$\vec{k}=\alpha_1\vec{b_1}+\alpha_2\vec{b_2} \tag{51}$$

The restriction set on wave vectors due to the periodic boundary conditions will serve useful in describing the linear combination coefficients α_i. In order to find such coefficients, equation (48) is solved:

$$\vec{k}\cdot\vec{a}_iN_i=2\pi m_i;\quad m_i\in\{0,1,2,\dots\}. \tag{52}$$

Another foundational equation is the relationship between the primitive vectors and the reciprocal space vectors is:

$$\vec{a_k}\cdot\vec{b_l}=2\pi\delta_{k,l}. \tag{53}$$

Applying this identity to equation (52):

$$\vec{k}\cdot\vec{a}_i=2\pi(\alpha_j\vec{b_j})\cdot\vec{a}_i=2\pi\alpha_j\delta_{i,j}. \tag{54}$$

Hence, the linear combination coefficients are restricted in value to:

$$\alpha_i=\frac{m_i}{N_i};\quad m_i\in\left[-\frac{N_i}{2},\frac{N_i}{2}\right]\wedge m_i\in Z. \tag{55}$$

Thus, the number of states is bounded by the size of the lattice, since N_i is the number of cells within a particular direction. Furthermore, whenever $m_i=N_i$, the wave vector will equal a point within the reciprocal lattice, $\vec{k}=\vec{G}$.

Therefore, all possible states of the lattice will be contained within a Wigner cell in reciprocal space. While this point will be fundamental in the description of the lattice's dynamics, it is first relevant to find the allowed angular frequencies.

At this point, the discussion now focuses on the case of Graphene. In order to find the allowed angular frequencies, it is necessary to find the Dynamical matrix, as revealed in equation (46). In the case of graphene, the Wigner cells take the shape of hexagons, which can be rotated to facilitate the definition of the primitive vectors:

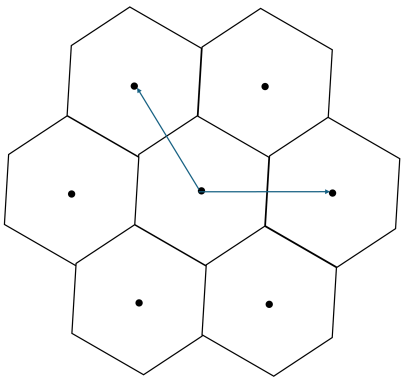

Fig. 2: Wigner Cells for Graphene

The decision to define the primitive vectors as those presented in figure 2 is based on the rotational symmetry of a hexagonal unit cell. When reflected once around the center of the cell, and if the primitive vectors are defined as those given previously, the six first neighbors will be correctly described. The primitive vectors in the Cartesian basis are hence given by:

$$\vec{a_1}=|a|(\hat{x}). \tag{56}$$

$$\vec{a_2}=|a|(-\frac{1}{2}\hat{x}+\frac{\sqrt{3}}{2}\hat{y}). \tag{57}$$

Having proposed a vibrational solution to the movement of each neighbor, it is possible to discover the shape of the dynamic matrix. To do so, Euler-Lagrange's equations of motion are once again utilized, finding a Kinetic term for the origin point and the Potential term in terms of its neighbors. This same methodology was previously applied for a generalized harmonic potential [2].

$$\sum_{\mu\nu\alpha}\sum_{\vec{k}\omega}-\omega^2m\varepsilon_\alpha\delta^{\mu\nu\alpha}_{\xi\eta\beta}\exp[-i(\vec{k}\cdot\vec{R_{\mu\nu}}-\omega\,t)]=\sum_{\xi\eta\beta}\sum_{\vec{k}\omega}D_{\alpha\beta}\varepsilon_\beta\exp[-i(\vec{k}\cdot\vec{R_{\xi\eta}}-\omega t)]. \tag{58}$$

It is desirable to solemnly focus on a single $\vec{k}$ before approaching the entire lattice. Therefore, the sum over all $\vec{k}$ is dropped momentarily. Furthermore, it is possible to bring both exponentials together by multiplying by $\exp[i(\vec{k}\cdot\vec{R_{\mu\nu}}-\omega t)]$:

$$-\sum_{\mu\nu\alpha}\omega^2m\varepsilon_\alpha\delta^{\mu\nu\alpha}_{\xi\eta\beta}+\sum_{\xi\eta\beta}D_{\alpha\beta}\varepsilon_\beta\exp[-i\vec{k}\cdot\vec{R_{\xi\eta}}+i\omega t+i\vec{k}\cdot\vec{R_{\mu\nu}}-i\omega t]=0. \tag{59}$$

Logically, it is possible to define a position vector from the origin to its neighbors:

$$\vec{R}_{\mu\nu\xi\eta} = \vec{R}_{\mu\nu} - \vec{R}_{\xi\eta} \tag{60}$$

By also assuming that the magnitude of the displacements of each element in the lattice is the same, $\varepsilon_\alpha = \varepsilon_\beta$, it is possible to express the equations of motion as:

$$\left[-\omega^2\delta^\alpha_\beta + \frac{1}{m}\sum_{\xi,\eta}^{NN} D^j{}_{\alpha,\beta}\exp[-i(\vec{k}\cdot\vec{R}_{\mu\nu\xi\eta})]\right]\varepsilon_\beta = 0. \tag{61}$$

The double summation in the kinetic term is effectively eliminated by the application of Kronecker's Delta: $\delta^{\mu\nu\alpha}_{\xi\eta\beta}$. Moreover, the analysis is reduced to only the nearest neighbors; an important characteristic of the relative position equation 60 is that, regardless of the choice of origin, it will always return the same position vectors.

Therefore, it is now possible to select an origin point, and obtain the relative position of its nearest neighbors, which will be the same for any origin point within the lattice. The simplest origin point is evidently: $\{\mu,\nu\}$=$\{0,0\}$; the label $j = \{\xi,\nu\}$ is introduced for simplicity. Having defined an origin, one may proceed to define a matrix, $\mathbf{D}$, which contains all the interaction-related information:

$$\mathbf{D} = \sum_j D^j_{\alpha,\beta}\exp[-i(\vec{k}\cdot\vec{R}_{00j})]\ . \tag{62}$$

Furthermore, one may find the list of first-neighbor relative positions from the origin:

$$\mathbf{R}_1 = \begin{pmatrix}1\\0\end{pmatrix},\quad \mathbf{R}_2 = \frac{1}{2}\begin{pmatrix}1\\\sqrt{3}\end{pmatrix},\quad \mathbf{R}_3 = -\frac{1}{2}\begin{pmatrix}1\\-\sqrt{3}\end{pmatrix},$$
$$\mathbf{R}_4 = -\mathbf{R}_1,\quad \mathbf{R}_5 = -\mathbf{R}_2,\quad \mathbf{R}_6 = -\mathbf{R}_3.$$

Having found the relative position from all six first neighbors, the main goal is to find the mathematical expression of the Dynamic Matrix (28). In this case,

$$D^j_{\alpha\beta} = \sum_{\xi'\eta'}^{NN} C_{\mu\nu\xi'\eta'}(\hat{R}_{\mu\nu\xi'\eta'\alpha}\hat{R}_{\mu\nu\xi'\eta'\beta})\delta^\mu_\xi\delta^\nu_\eta - C_{\mu\nu\xi'\eta'}\hat{R}_{\mu\nu\xi\eta\alpha}\hat{R}_{\mu\nu\xi\eta\beta}, \tag{63}$$

where *NN* denotes nearest neighbors. Rearranging, equation (63) can be written as

$$D^j_{\alpha\beta} = \sum_{j=1}^{6} C_j(\hat{R}_{j\alpha}\hat{R}_{j\beta})\delta^\mu_\xi\delta^\nu_\eta - C_j\hat{R}_{00j\alpha}\hat{R}_{00j\beta}. \tag{64}$$

The interaction matrix $\mathbf{D}$ will then be given by:

$$\mathbf{D}_{\alpha,\beta} = \sum_j\left\{\left[\sum_j C\hat{R}_{00j\alpha}\hat{R}_{00j\beta}\right]\delta^\mu_\xi\delta^\nu_\eta - C\hat{R}_{00j\alpha}\hat{R}_{00j\beta}\right\}\exp\left[-i(\vec{k}\cdot\vec{R}_{00j})\right]. \tag{65}$$

By applying the choice of origin, the expression can be further simplified to:

$$D^j_{\alpha\beta} = \sum_j A_{\alpha\beta}\delta^0_j\exp\left[-i\left(\vec{k}\cdot\vec{R}_{00j}\right)\right] - \sum_j C\hat{R}_{00j\alpha}\hat{R}_{00j\beta}\exp\left[-i\left(\vec{k}\cdot\vec{R}_{00j}\right)\right] = A_{\alpha\beta} - Z_{\alpha\beta}. \tag{66}$$

Auxiliary tensors may be defined, which will simplify symbolic evaluation. These tensors are defined as $A_{\alpha\beta}$ and $Z_{\alpha\beta}$. The remaining steps are fully computational, and require the evaluation of the auxiliary tensors on every possible permutation of components:

$$A_{\alpha\beta} = \left[\sum_j C_j\hat{R}_{00j\alpha}\hat{R}_{00j\beta}\right]. \tag{67}$$

This expression is evaluated for the three possible component combinations, noticing the symmetric nature of $\{x,y\} = \{y,x\}$:

$$A_{xx} = \sum_{j=1}^{6} C_j\hat{R}_{0,0,j,x}\hat{R}_{0,0,j,x}, \tag{68}$$

$$A_{yy} = \sum_{j=1}^{6} C_j\hat{R}_{0,0,j,y}\hat{R}_{0,0,j,y}, \tag{69}$$

$$A_{xy} = A_{yx} = \sum_{j=1}^{6} C_j\hat{R}_{0,0,j,x}\hat{R}_{0,\,0,j,y}. \tag{70}$$

Furthermore, the other auxiliary tensor is evaluated on the three distinct permutations:

$$Z_{\alpha,\beta} = \sum_j C_j\hat{R}_{0,0,j,\alpha}\hat{R}_{0,\,0,j,\beta}\exp[-i(\vec{k}\cdot\vec{R}_{00j})], \tag{71}$$

$$Z_{xx} = \sum_j C_j\hat{R}_{0,0,j,x}\hat{R}_{0,0,j,\,x}\exp[-i(\vec{k}\cdot\vec{R}_{00j})], \tag{72}$$

$$Z_{xy} = Z_{yx} = \sum_j C_j\hat{R}_{0,0,j,x}\hat{R}_{0,0,j,y}\ \exp[-i(\vec{k}\cdot\vec{R}_{00j})], \tag{73}$$

$$Z_{yy} = \sum_j C_j\hat{R}_{0,0,j,x}\hat{R}_{0,0,j,\,y}\exp[-i(\vec{k}\cdot\vec{R}_{00j})]. \tag{74}$$

Using these results, the assembly of the interaction matrix $\mathbf{D}$ is computationally efficient. In order to obtain each of the four components of the 2D $\mathbf{D}$, one simply evaluates:

$$D = A_{\alpha,\beta} - Z_{\alpha,\beta}, \tag{75}$$

$$D_{12} = D_{21} = A_{xy} - Z_{xy}, \tag{76}$$

$$D_{22} = A_{yy} - Z_{yy}. \tag{77}$$

The interaction matrix has a complicated mathematical form, even for the nearest neighbors. For that reason, it proves useful to evaluate the different coefficients C_j, each unique to one of the six neighbors:

$$C_1 = C_4 = \frac{245}{2}, \tag{78}$$

$$C_2 = C_5 = \frac{245}{8}, \tag{79}$$

$$C_3 = C_6 = \frac{735}{8}. \tag{80}$$

These values correspond to the values used by Sahoo in his analysis of embedded Graphene structures [3]. By choosing these coefficients, it is possible to simplify the shape of the interaction matrix for first neighbors to:

$$D_{11} = -\frac{245}{16}\left(-20+16\cos(k_x)+3\cos\left(\frac{1}{2}(k_x-\sqrt{3}k_y)\right)+\cos\left(\frac{1}{2}(k_x+\sqrt{3}k_y)\right)\right),$$

$$D_{12} = -\frac{245}{16}\sqrt{3}\left(2-3\cos\left(\frac{1}{2}(k_x-\sqrt{3}k_y)\right)+\cos\left(\frac{1}{2}(k_x+\sqrt{3}k_y)\right)\right),$$

$$D_{21} = -\frac{245}{16}\sqrt{3}\left(2-3\cos\left(\frac{1}{2}(k_x-\sqrt{3}k_y)\right)+\cos\left(\frac{1}{2}(k_x+\sqrt{3}k_y)\right)\right),$$

$$D_{22} = -\frac{735}{16}\left(-4+3\cos\left(\frac{1}{2}(k_x-\sqrt{3}k_y)\right)+\cos\left(\frac{1}{2}(k_x+\sqrt{3}k_y)\right)\right).$$

The interaction matrix has purely real components and is symmetric in nature, so it is therefore Hermitian. The reason behind the realness of the interaction matrix is the embedded symmetry of hexagonal lattices; as previously discussed, the selected choice of primitive vectors allows for a reflection of the first three nearest neighbors that successfully recovers the remaining three. A Hermitian matrix is guaranteed to have real eigenvalues; in this case, the eigenvalues obtained using the characteristic equation will provide the dispersion relation of the material:

$$\mathbf{det}\left[-\omega^2\hat{I}+\frac{1}{m}D\right]=0. \tag{81}$$

For the nearest neighbors, there will be two distinct eigenvalues ω^2. Therefore, there will exist four values of ω; however, there are only two unique values of ω, which are presumed to represent the acoustic and optical dispersion relations within Graphene.

A phonon is a bosonic pseudoparticle, and corresponds to the quantization of the vibrational modes in a material's structure. Acoustic phonons are related to lower energy vibrational elements in the lattice, while optical phonons correspond to more energetic interactions. While acoustic phonons mediate thermal conductivity within the material, optical phonons mediate phonon-photon interactions in the lattice. The results section will feature the two distinct dispersion relations, namely ω_1, ω_4, which correspond to acoustic and optical modes respectively [4].

e. Ising model

One of the main tenets of statistical physics and phase transition theory is the Ising model, which offers a profound comprehension of how microscopic interactions may result in aggregate macroscopic behaviors.

Mathematically, itl considers a lattice of dimension d, where each site i is occupied by a spin variable s_i that can take one of two possible values: $s_i = +1$ or $s_i = -1$. These values represent the two possible states of an elementary magnetic dipole: oriented up or down. The interaction between neighboring spins and the influence of an external magnetic field are incorporated into the Hamiltonian of the system, which describes its total energy [5].

The Hamiltonian H of the Ising model is expressed as:

$$H = -J\sum_{\langle i,j\rangle} s_i s_j - h\sum_i s_i, \tag{82}$$

where $\langle i,j\rangle$ indicates that the sum is taken across all pairs of nearby spins in the lattice, whereas J is the exchange constant that measures the amount of interaction between surrounding spins s_i and s_j in this equation. An external magnetic field that is evenly applied to all spins is denoted by the word h. If $J > 0$, the interaction is ferromagnetic, meaning that the spins prefer to align in the same direction to reduce the energy of the system, as shown by the negative sign in the interaction term.

Next, the partition function Z allows us to calculate the thermodynamic parameters of the system. Its definition is the total of all conceivable spin configurations' probability, weighted by the Boltzmann factor:

$$Z = \sum_{\{s_i\}} e^{-\beta H}. \tag{83}$$

where $\beta = \frac{1}{k_B T}$, with k_B being the Boltzmann constant and T the absolute temperature. The sum $\sum_{\{s_i\}}$ extends over all possible spin configurations $\{s_i\}$, of which there are 2^N for a system with N sites.

The Helmholtz free energy F is related to the partition function through:

$$F = -k_B T \ln Z. \tag{84}$$

This connection is essential because it makes it possible to deduce other thermodynamic characteristics using derivatives of F with regard to the pertinent parameters. As an illustration, the average magnetization $\langle M\rangle$, a measurement of the system's magnetic order, may be found as follows:

$$\langle M\rangle = -\left(\frac{\partial F}{\partial h}\right)_T = \frac{1}{Z}\sum_{\{s_i\}}\left(\sum_i s_i\right)e^{-\beta H}. \tag{85}$$

The system's reaction to an external magnetic field is measured by the magnetic susceptibility χ, which may be computed as follows:

$$\chi = \left(\frac{\partial\langle M\rangle}{\partial h}\right)_T = \beta\left(\langle M^2\rangle - \langle M\rangle^2\right). \tag{86}$$

The specific heat C is related to energy fluctuations and is defined as:

$$C = \left(\frac{\partial\langle E\rangle}{\partial T}\right)_h = \frac{\beta^2}{N}\left(\langle E^2\rangle - \langle E\rangle^2\right). \tag{87}$$

where $\langle E \rangle$ is the average energy of the system [6].

The critical behavior of the Ising model close to the critical temperature T_c, when a second-order phase shift takes place, is among its most fascinating features. A sudden change in the magnetization of the system and the appearance of long-range correlations between the spins are characteristics of this transition.

It is shown that the Ising model does not show a phase transition at finite temperature and that it may be solved exactly in one dimension (1D). In this instance, the transfer matrix approach is used to compute the partition function. The transfer matrix $\mathbf{T}$ is defined using the following elements:

$$T_{s_i,s_{i+1}} = e^{\beta J s_i s_{i+1} + \beta h s_i}. \tag{88}$$

The partition function is then expressed as:

$$Z = \mathrm{Tr}(\mathbf{T}^N). \tag{89}$$

where N is the number of sites and Tr denotes the trace of the matrix. The eigenvalues of $\mathbf{T}$ determine the thermodynamic behavior of the system.

The correlation length and magnetic susceptibility divergence define the crucial behavior close to T_c. The correlation between spin fluctuations at one site and those at another site r away is measured by the spin correlation function $G(r)$:

$$G(r) = \langle s_i s_{i+r} \rangle - \langle s_i \rangle \langle s_{i+r} \rangle. \tag{90}$$

Near T_c, $G(r)$ decays as a power law:

$$G(r) \sim \frac{e^{-r/\xi}}{r^{\eta}}. \tag{91}$$

where ξ is the correlation length, which diverges as $\xi \sim |T - T_c|^{-\nu}$, and η is the correlation exponent. In 2D, the critical exponents take the exact values $\nu = 1$ and $\eta = \frac{1}{4}$.

The Ising model cannot be solved exactly in dimensions larger than two, although approximations like mean field theory and the renormalization group can be used. According to mean field theory, the system's average magnetization causes each spin to experience an effective field. When there is no external field present, the magnetization's self-consistent equation is [6]:

$$M = \tanh\left(\frac{JzM}{k_B T}\right). \tag{92}$$

where z is the number of nearest neighbors in the lattice. The critical temperature in the mean field approximation is obtained by linearizing this equation near $M = 0$:

$$k_B T_c^{\mathrm{MF}} = Jz. \tag{93}$$

Mean field theory does not give the right critical exponents for low dimensions, but it does qualitatively represent the existence of a phase transition. Kenneth Wilson and others invented the renormalization group, a technique that gives us a powerful tool to systematically determine critical exponents and helps us understand how interactions change as the length scale changes.

Studying the Ising model in dimensions without precise solutions requires the use of Monte Carlo simulations. Using a criterion derived from the Boltzmann factor, the Metropolis algorithm, one of the most popular, generates spin configurations through random modifications that are either approved or rejected. This enables us to examine the system's crucial behavior and estimate thermodynamic properties numerically [6].

III. Results

a. Lattice Specific Heat

In previous sections, two distinct dispersion relations were defined, $\omega_1(\vec{k}), \omega_4(\vec{k})$. Although their mathematical form remains complicated, it is possible to plot the dispersion relations in a 3D surface plot:

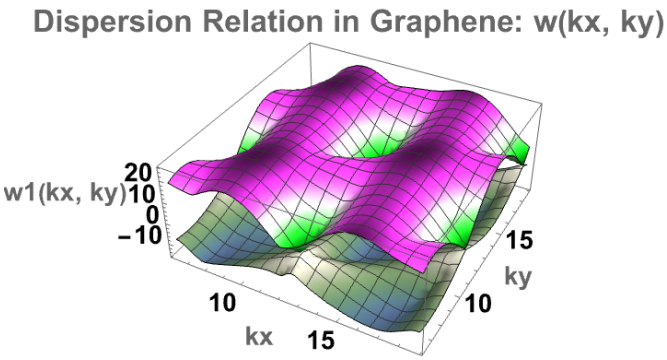

Fig. 3: The dispersion relation for Graphene's first neighbors

To further analyze the two dispersion curves, a surface level is analyzed such that $k_y = 0\ \forall k_x$:

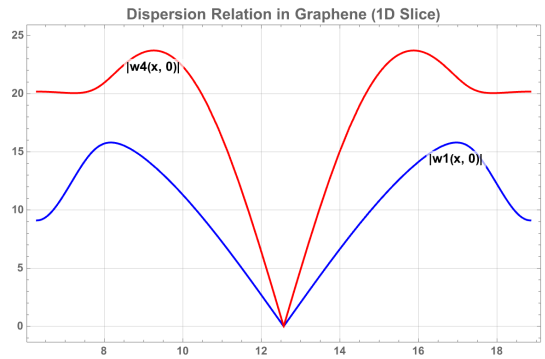

Fig. 4: The dispersion relation for Graphene's first neighbors

Clearly, ω_1 is related to the acoustic phonons within the lattice, while ω_4 appears to be related with the more energetic optical phonons. At this point, it is possible to obtain the internal energy within the lattice. For this purpose, Sahoo's internal energy model is revisited:

$$U = \sum_s \sum_{\vec{k}} \frac{h\omega_s(\vec{k})}{(2\pi)^4 (e^{\frac{h\omega_s(\vec{k})}{2\pi k_B T}} - 1)}. \tag{94}$$

In this case, the dispersion relations are evaluated over the allowed wave vectors found using the Born-Von Kármán

boundary conditions in a 50 x 50 lattice of neighbors. These evaluations are summed for each of the two ω, hence considering both the acoustic and optical phonon contributions.

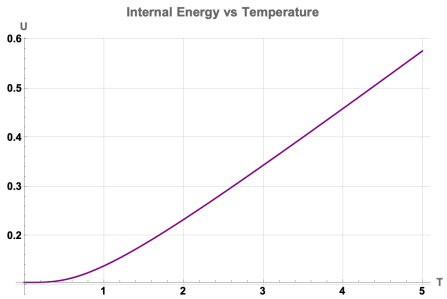

Fig. 5: The internal energy for Graphene's first neighbors

Finally, it is possible to derive the internal energy expression and obtain the specific heat of the Graphene lattice:

$$\frac{\partial U}{\partial T} = C_V \tag{95}$$

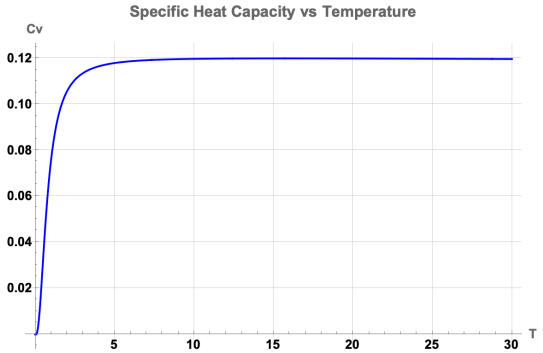

Fig. 6: The specific heat for Graphene up to first neighbor interactions **Dimensionless analysis*

For lower temperature values, the cubic behavior commonly found experimentally is replicated [7]:

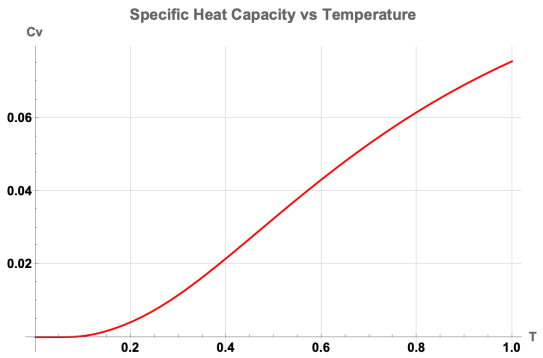

Fig. 7: The specific heat for Graphene up to first neighbor interactions **Dimensionless analysis*

Even though this initial analysis effectively replicates the expected behavior at low temperatures, it is possible to improve the analysis by considering a higher number of neighbor interactions.

There are twelve second neighbors for each point within the lattice. Once again, it proves useful to select $\{0,0\}$ as the origin point. Then, the relative position of the twelve second neighbors will be given by [8]:

$$\begin{aligned}
&\mathbf{M}_1 = 2\mathbf{R}_1, \quad \mathbf{M}_2 = 2\mathbf{R}_1 + \mathbf{R}_3, \quad \mathbf{M}_3 = 2\mathbf{R}_2, \\
&\mathbf{M}_4 = 2\mathbf{R}_3 + \mathbf{R}_1, \quad \mathbf{M}_5 = 2\mathbf{R}_3, \quad \mathbf{M}_6 = -2\mathbf{R}_1 + \mathbf{R}_3, \\
&\mathbf{M}_7 = -\mathbf{M}_1, \quad \mathbf{M}_8 = -\mathbf{M}_2, \quad \mathbf{M}_9 = -\mathbf{M}_3, \\
&\mathbf{M}_{10} = -\mathbf{M}_4, \quad \mathbf{M}_{11} = -\mathbf{M}_5, \quad \mathbf{M}_{12} = -\mathbf{M}_6.
\end{aligned}$$

Once again, the interaction matrix may be constructed using the two auxiliary matrices $D = A_{\alpha,\beta} - Z_{\alpha,\beta}$:

$$A_{\alpha,\beta} = \left[\sum_{j}^{SN} C_j \hat{R}_{0,0,j,\alpha} \hat{R}_{0,0,j,\beta}\right] \tag{96}$$

$$Z_{\alpha,\beta} = \sum_{j}^{SN} C_j \hat{R}_{0,0,j,\alpha} \hat{R}_{0,\,0,j,\beta} \exp[-i(\vec{k} \cdot \vec{R_{00}}_j)] \tag{97}$$

The only key difference between the first approximation is that the summation now round through 18 different neighbors (six first and twelve second neighbors). Once again, the mathematical form of the interaction matrix is complicated, so it will be presented symbolically as **D** (the symbolic evaluation is added in the attachments). The selected coefficients are chosen based on Sahoo's work [3]:

$$C_1 = C_4 = \frac{245}{2}, \tag{98}$$

$$C_2 = C_5 = \frac{245}{8}, \tag{99}$$

$$C_3 = C_6 = \frac{735}{8}, \tag{100}$$

$$C_k = 100 \;\forall\; k \geq 7. \tag{101}$$

Once more, two different dispersion relations are obtained. There are important differences between both models, as can be perceived from the surface plot:

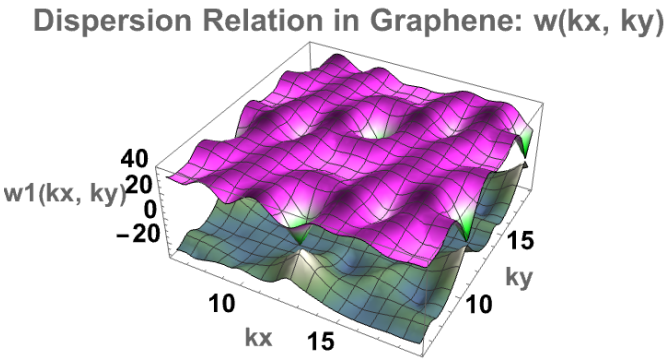

Fig. 8: The dispersion relation for Graphene's second neighbors

A similar level surface cut can be plotted to further analyze the dispersion relations. The main difference between both models is the accuracy of energetic vibrational modes. This will improve the results for both the internal energy and the specific heat at low temperatures.

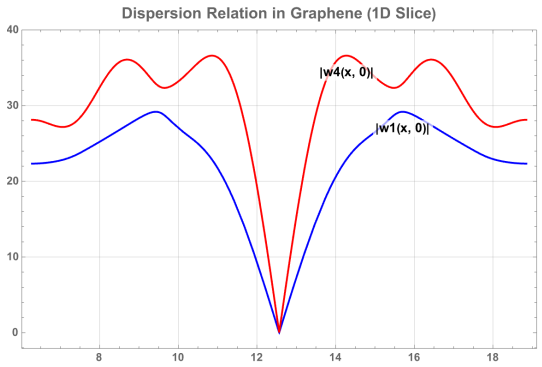

Fig. 9: The dispersion relation for Graphene's second neighbors

The internal energy is once again calculated using equation 94. The lattice remains 50 x 50, obtaining the following results:

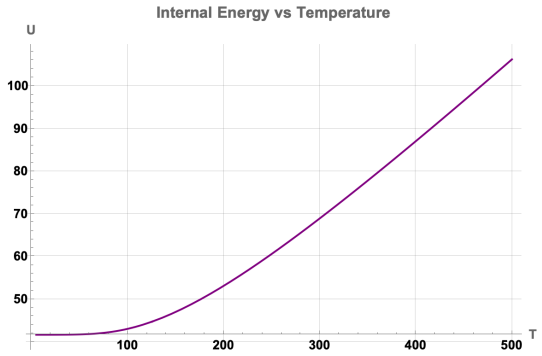

Fig. 10: The internal energy for Graphene's second neighbors

Finally, the specific heat of the lattice is calculated by taking the derivative of the internal energy expression:

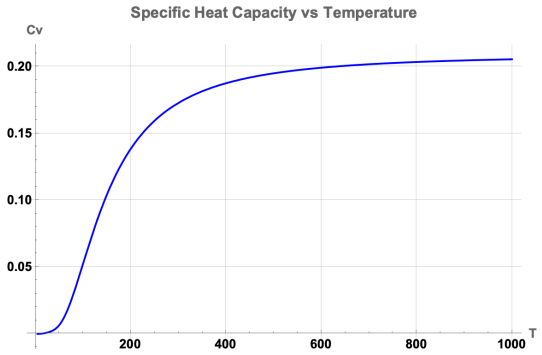

Fig. 11: The internal energy for Graphene's second neighbors

For low temperatures, the cubic behavior is once again recovered and further improved when compared to the first results. It is now possible to explore the magnetic specific heat, which was explored numerically through an Ising Model. With the result of the present section and the one presented next, a complete characterization of the material's specific heat will be available.

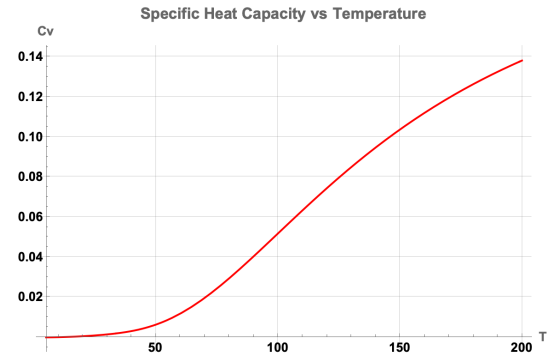

Fig. 12: The internal energy for Graphene's second neighbors

b. Ising model and Magnetic Specific Heat

This Ising model simulation featured a three-neighbor interaction network to model graphene with 3000×3000 nodes, resulting in a square lattice of 9 million elements with periodic boundaries, as it is shown in Fig.13. The primary goal of the simulation was to explore the thermodynamic behavior of the system, particularly the dependence of internal energy and specific heat on temperature.

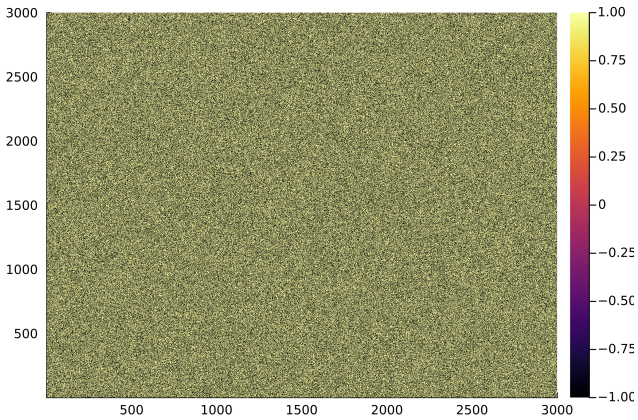

Fig. 13: Graphene spin grid

To analyze the system's relaxation dynamics, the evolution of energy through Monte Carlo steps was examined for two distinct temperatures: $T_1 = 2{,}0 \wedge T_2 = 15{,}0$. Once it was assured that the system reached equilibrium, temperature was decreased so that the dimensionless internal energy was calculated as a function of temperature.

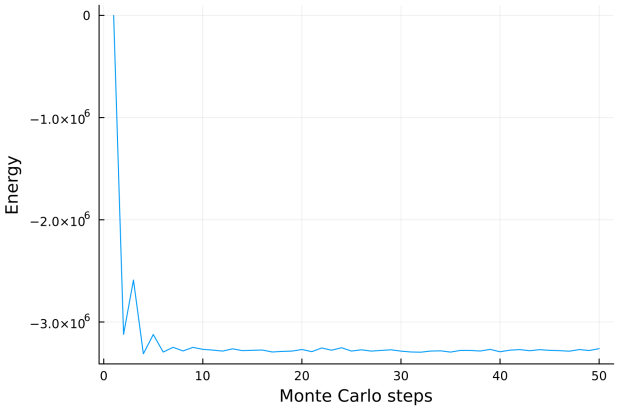

Fig. 14: Energy with respect to Monte Carlo steps for a stationary state, $T = 15{,}0$

On the first place, we observe in Fig.14 an exponential decay with some local peaks, specially at the beginning.

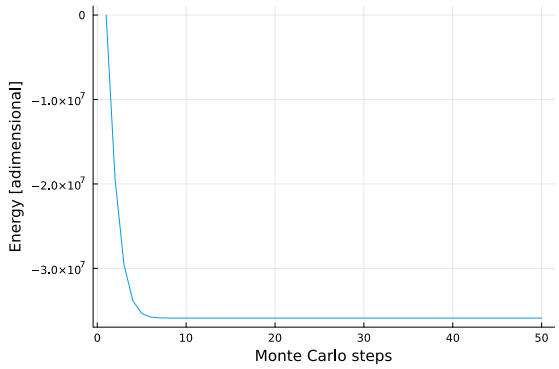

Fig. 15: Energy with respect to Monte Carlo steps for a stationary state, $T = 2{,}0$

On the other hand, when modelling the system with temperature $T = 2{,}0$, we observe in Fig.21 a smoother decay, with a lower order of magnitude in the energy.

This work's goal was to analyze the specific heat for both lattice and magnetic interactions. We reached this quantity by applying a numerical derivative to the data obtained in Figs.14 and 21.

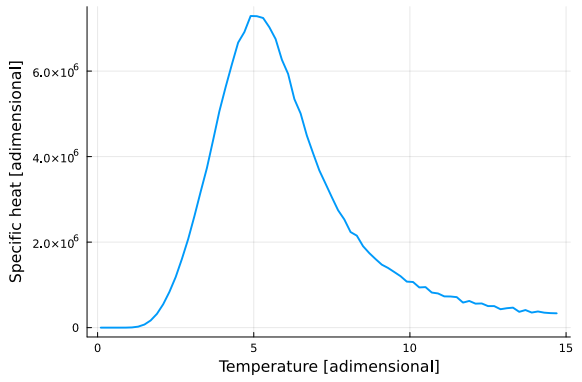

Fig. 16: Specific heat with respect to temperature, $T = 15{,}0$

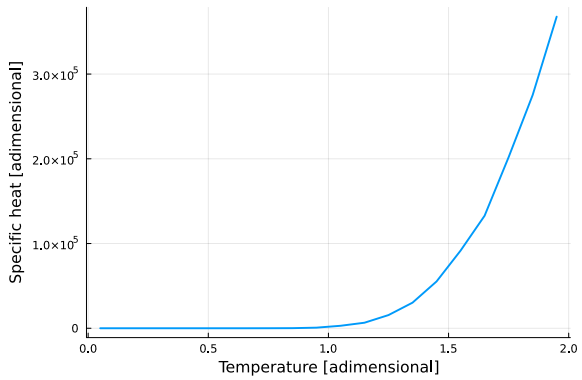

Fig. 17: Specific heat with respect to temperature, $T = 2{,}0$

As we can appreciate in Figs.16 and 17, the specific heat due to magnetic interactions was clearly lower at higher temperatures as the magnetic fields lose intensity the hotter a system is. It reached a peak around the system's critical temperature. Further simulation was done near the zero temperature that showed a smooth decay analogic to that of a Debye's model.

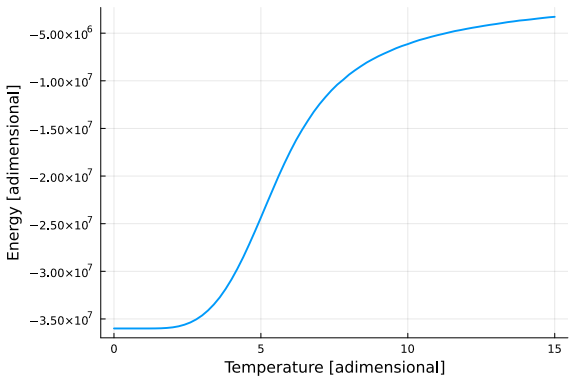

Fig. 18: Internal energy with respect to temperature, $T = 15{,}0$

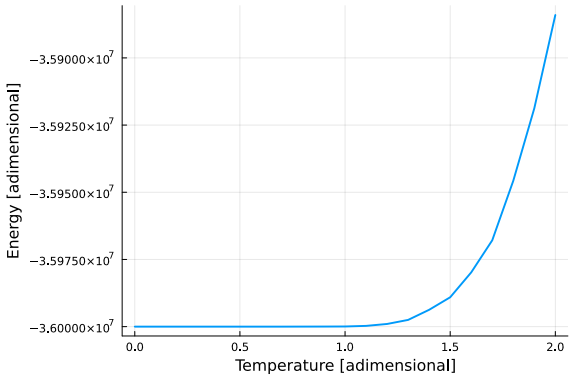

Fig. 19: Internal energy with respect to temperature, $T = 2{,}0$

With respect to the internal, for high temperatures, it tends to a constant, as shown in Fig.18. By contrast, when we are in low temperatures, Fig.19, it decreases exponentially, tending to a very negative value.

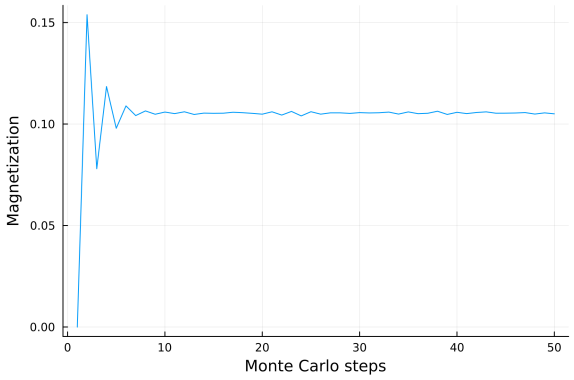

Fig. 20: Magnetization with respect to Monte Carlo steps,$T = 15{,}0$

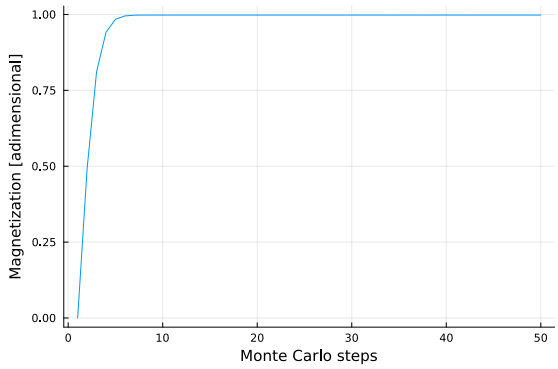

Fig. 21: Magnetization with respect to Monte Carlo steps, $T = 2{,}0$

Finally, we can appreciate in Fig.20 that as the Monte Carlo step progresses, the magnetization value tends to a constant of 0,10, showing some local peaks at the first iterations. Meanwhile, Fig.21 shows that for low temperatures, it quickly converges to 1.0 for almost all the simulation.

IV. Future work and the magnetocaloric effect

In this section, we will generate a brief discussion on a possible application for graphene in the medical field through cancer treatments which utilize the magnetocaloric effect. This is a novel application of graphene alloy structure, and could be benefitted by our in depth model of graphene's specific heat.

New research has demonstrated extreme potential for the utilization of the magnetocaloric effect in the treatment of cancer. Magnetic hyperthermia is the name given to a medical procedure in which magnetic nanoparticles are inserted into a patient's body and guided to a cancerogenous tumor. When in the tumor, the patient is exposed to a magnetic field, which induces the magnetocaloric effect in these particles. This causes a localized temperature rise and can lead to the tumors eradication by apoptosis due to the high temperature without harming any healthy tissue. [9]

Currently, the ferromagnetic materials utilized typically consist of magnetite and maghemite, two ferromagnetic iron oxides. Having a low specific heat spectrum (between 0.6 and 1 J/gK) these materials are ideal as the temperature increase is more drastic. Graphene's lower specific heat could be utilized in these types of procedures in combination with the magnetite and maghemite to create more optimal nanoparticles for this procedure. Due to graphene's lower specific heat, the resulting alloy between this and the ferromagnetic materials previously mentioned would result in a lower overall specific heat when compared to the individual ferromagnetic materials. A combination of this nature would ensure both the ferromagnetic properties required for the magnetocaloric effect's presence and a lower specific heat to increase temperature change in the material and, consequently, the tumor in question. [10]

Graphene's lower specific heat would not be the only benefit endorsing the integration of this material into the ferromagnetic nanoparticles. Due to the hexagonal structure of graphene its heat dissipation is extremely efficient and effective. This property could be utilized to ensure that no unwanted localized hot and cold spots inside the tumor are created. Following this same nature, magnetic nanoparticles tend to agglomerate which again can lead to an uneven heat distribution in the tumor. Graphene's electrostatic properties can be utilized in order to equally disperse the ferromagnetic nanoparticles and ensure a proper temperature rise in the tumor.

Future research is required to determine the effectiveness of these theoretical altered nanoparticles when compared to the already utilized completely ferromagnetic nanoparticles. A combination of graphene and iron oxides would result in an alteration of all the nanoparticles' properties. This could in turn lead to unforeseen unwanted results. Another thing to consider is the biocompatibility of the material. The graphene utilized in this process would require certain alteration in order to increase its biocompatibility as pristine graphene can cause oxidative stress, inflammation, and damage to cellular membranes due to its sharp edges and strong interactions with cell membranes. The necessary modifications to the graphene could possibly cause alteration to its structure and affect the properties previously discussed in this section. [11]

Finally, future research on this topic would not only serve to expand the scientific knowledge of this topic but also possibly serve as a mayor breakthrough in non-invasive cancer treatment.

V. Conclusions

Throughout this document we have presented a detailed methodology with the aim of obtaining the specific heat for graphene and its lattice. We have successfully produced results and were able to obtain a graph depicting the behavior of this material's specific heat and its values for different temperatures.

The next necessary improvements involve a higher neighbor interaction approximation, as well as a dimensional analysis of the units involved in the calculation. In order to correctly join both the phonon specific heat and the magnetic specific heat, both simulations should contain a similar number of cells within the lattice. This step was particularly challenging throughout the symbolic evaluation of neighbor interactions, limiting the size of the lattice.

Furthermore, it is relevant to study the specific heat of graphene alloys, as well as present a variety of results for different strengths of the external magnetic field. Experimental research should be performed alongside the mathematical models here presented, further validating the veracity of the results.

References

[1] R. Sahoo and R. R. Mishra, "Lattice Specific Heat of Graphene," in *Fourth International Conference on De-*

vices, Circuits and Systems (ICDCS'18). IEEE, 2018, pp. 186–188.

[2] H. Goldstein, C. Poole, and J. Safko, *Classical Mechanics*, 3rd ed. Addison-Wesley, 2002.

[3] R. Sahoo, "Phonon Dispersion of Graphene Revisited," *Journal of Experimental and Theoretical Physics*, vol. 114, no. 5, pp. 805–809, 2012.

[4] C. Kittel, *Introduction to Solid State Physics*, 8th ed. John Wiley & Sons, 2005.

[5] J. S. Walker, *A Student's Guide to the Ising Model*. Cambridge University Press, 2023.

[6] T. T. Wu and B. M. McCoy, *The Two-Dimensional Ising Model*. Harvard University Press, 1973.

[7] S. Mann, P. Rani, G. S. Dubey, and V. K. Jindal, "Thermodynamic properties of pure and doped (b, n) graphene," *RSC Advances*, vol. 6, pp. 9025–9033, 2016.

[8] L. Falkovsky, "Phonon dispersion in Graphene," *Journal of Experimental and Theoretical Physics*, vol. 105, no. 2, pp. 397–403, 2007.

[9] X. Liu, Y. Zhang, Y. Wang, W. Zhu, G. Li, X. Ma, Y. Zhang, S. Chen, S. Tiwari, K. Shi, S. Zhang, H. M. Fan, Y. X. Zhao, and X. J. Liang, "Comprehensive understanding of magnetic hyperthermia for improving antitumor therapeutic efficacy," *Theranostics*, vol. 10, no. 8, pp. 3793–3815, Feb 2020.

[10] J. M. Cowley, "An approximate theory of order in alloys," *Physical Review*, vol. 77, no. 6, pp. 669–675, March 1950.

[11] C. Liao, Y. Li, and S. C. Tjong, "Graphene nanomaterials: Synthesis, biocompatibility, and cytotoxicity," *International Journal of Molecular Sciences*, vol. 19, no. 11, p. 3564, Nov 2018.